

## THE DRAG COEFFICIENT OF FINITE-ASPECT-RATIO PERFORATED CIRCULAR CYLINDERS

T.R. ALRIDGE, B.S. PIPER and J.C.R. HUNT

University of Cambridge Engineering Department, Trumpington Street, Cambridge  
CB2 1 PZ (Gt. Britain)

(Received October 20, 1977)

### Summary

Measurements are described of the drag coefficient of porous circular cylinders (60% open-area ratio) fixed between solid hemispherical end caps, for five values of aspect ratio between 7.92 and 2.67. The Reynolds number varies between  $10^4$  and  $2.6 \times 10^5$ . It is found that the drag coefficient increases with aspect ratio much as a solid cylinder's but its drag coefficient is about 20% higher (varying between 0.88 to 0.96 as the aspect ratio is increased).

Flow-visualization experiments have also been conducted, and show how fluid passes through the cylinders and how the vortex shedding is weaker than for solid cylinders.

### 1. Introduction

It is well known that perforating, or rendering porous, a fence normal to the flow *reduces* its drag, but increases its effect on the flow further downwind, i.e. lengthens its effective wake [1,2]. It is less well known that perforating a solid body *increases* its drag, and reduces its tendency to shed strong vortices. Both of these properties were used in the design of the aerodynamic dampers which the Central Electricity Generating Board in England uses to attach to overhead high-tension cables to reduce the amplitude of wind-induced galloping motions [3] (see Fig. 1). In the design of these dampers which are essentially perforated circular cylinders with aspect ratio 4.23 and 60% open-area ratio, in the absence of any data, the drag coefficient was assumed to be about 1.5. The first object of the tests reported here was

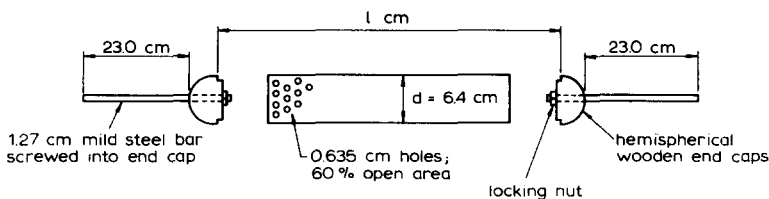


Fig. 1. Exploded view of the perforated cylinder, the solid end caps and the supporting bar.

to measure the drag coefficient of these dampers for various aspect ratios.

The reduction of vortex shedding by perforating a cylinder or sphere is used in the design of perforated cylindrical shrouds to reduce vortex shedding by chimneys or other cylindrical structures [4] and in the design of a gust recorder which measures the forces on a perforated sphere [5]. In the second part of this experiment we used flow-visualization studies to look for causes of the increase in drag and reduction in vortex shedding when a cylinder becomes porous.

## 2. Apparatus

### 2.1 Perforated cylinder

A perforated cylinder (see Figs. 1, 2) was made from mild steel plate 0.17" thick, perforated with 0.63 cm holes at 0.95 cm equilateral centres, giving 40.3% covered area. This plate was rolled into a 6.40 cm cylinder, with diameter ( $d$ ) (= 6.40 cm) and length  $l$ . The plate was spot welded along the overlap

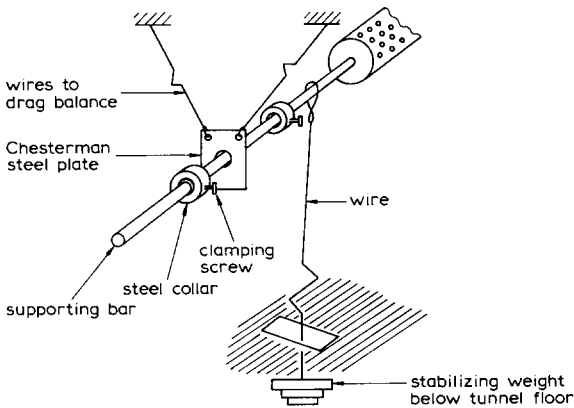


Fig. 2. Connections between the supporting bar and the wires attached to the drag balance and the stabilizing weight.

at frequent intervals. The length  $l$  was initially 50.7 cm and for each subsequent test was shortened until in test 5 it was 17.1 cm. Wooden end caps were then made to fit the cylinder. They were hemispherical with insets as shown in Fig. 1, Section 3.1, with a diameter of 6.40 cm.

Half-inch holes were then drilled and tapped in the end caps to take the 1.25-cm-diameter mild-steel supporting bars which screwed into them. A locking nut was placed for safety on the ends of the supporting bars. The end caps were then fixed to the cylinder by means of screws through the perforations.

### 2.2 Wind tunnel

The supporting bars were supported by Chesterman steel plates which were

attached to 2 wires from the drag balance and a wire to a stabilizing weight below the wind-tunnel floor. The drag measurements on the aerodynamic dampers were made in the 1.20 m  $\times$  1.5 m closed return wind tunnel in the Cambridge University Engineering Department. The wind speed  $U$  was calculated from pressure measurements across the wind-tunnel contraction.

Flow-visualization studies were conducted on the 7.92 aspect-ratio cylinders in the wind tunnel by (a) observing the motion of wool tufts attached to (i) the surface of the cylinder and (ii) to a rod moved around in the wake at the highest Reynolds number ( $Ud/\nu$ ) of  $1.2 \times 10^5$ , and (b) by injecting smoke upstream of the cylinders and into the wake at a Reynolds number of only 3000. Visualization studies were also conducted on the flow through a section of the cylinder (about one diameter long) in a slow-moving-water channel (Reynolds number of about 3000).

### 3. Results

#### 3.1 Drag

The aspect ratio of the cylinder was defined to be the ratio of the length ( $l$ ) of the perforated cylindrical section of the damper to the diameter ( $d$ ). The drag of the aerodynamic damper and its supporting bar ( $D_{AB}$ ) was measured for five values of  $l/d$ . For each value of  $l$ , the Reynolds number ( $Re$ ) was varied from about  $10^4$  to nearly  $2 \times 10^5$ . Typical results for the ratio  $D_{AB}/U^2$  are plotted in Fig. 3 showing the large scatter ( $\pm 10\%$ ) when  $Re < 5 \times 10^4$ , but much smaller scatter ( $\pm 2\%$ ) when  $Re > 5 \times 10^4$ .

When these tests were finished, the drag  $D_B$  of a circular bar (1.25 cm diameter and 46 cm long) with the *same* fitting attachments and wires was measured (test 6). The drag coefficient was found to be 1.43 (based on the bar diameter) with less than 3% variation as  $Re$  was varied from  $7 \times 10^3$  to

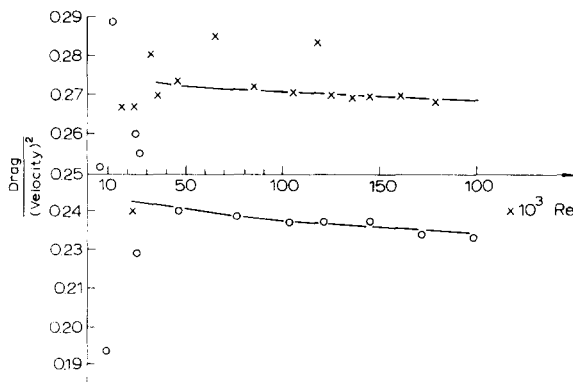


Fig. 3. Measurements of drag/(velocity)<sup>2</sup> ( $D_{AB}/U^2$ ) (in  $N m^{-2} s^2$ ) plotted as a function of  $Re$  to show large scatter at  $Re < 5 \times 10^4$ .  $\times$  Test 1, aspect ratio 7.92;  $\circ$  Test 2, aspect ratio 6.50.

$5.2 \times 10^4$ . This drag ( $D_B$ ) varies between a fifth (test 1) and a third (test 5) of the total drag  $D_{AB}$ .

The drag was also measured of the two hemispherical end caps and the supporting bar ( $D_{CB}$ ) (test 7).  $D_{CB}$  is about one half  $D_{AB}$ .

From these tests, the drag of the aerodynamic damper  $D_A$  was estimated, assuming that the drag of the damper and the supporting bars are independent of each other, so that

$$D_A = D_{AB} - D_B. \quad (1)$$

Using the projected area  $\delta$  of the damper, excluding the supporting bar, we calculate  $C_D$ . In Table 1, the values of  $C_D$  are given at the extreme ends of

TABLE 1

Net drag coefficient of aerodynamic dampers  $C_{DA}$ 

Test	Aspect ratio ( $l/d$ )	$C_D$ (mean values at extremes of $Re$ )	$Re$ range	Scatter
1	7.92	0.965 → 0.944	$4.3 \times 10^4 \rightarrow 1.72 \times 10^4$	$\pm 0.024$
2	6.50	0.974 → 0.924	$4.52 \times 10^4 \rightarrow 2.24 \times 10^4$	$\pm 0.01$
3	5.45	0.921 → 0.897	$4.3 \times 10^4 \rightarrow 20.9 \times 10^4$	
4	4.02	0.909 → 0.887	$4.3 \times 10^4 \rightarrow 23.2 \times 10^4$	
5	2.67	0.882 → 0.855	$4.3 \times 10^4 \rightarrow 26.2 \times 10^4$	
6	(bar, wires)	1.43	$7.1 \times 10^3 \rightarrow 5.2 \times 10^4$	$\pm 0.03$
7	(bar, end caps, wires)	0.48	$5 \times 10^4 \rightarrow 23 \times 10^4$	$\pm 0.01$

Note: (i)  $l$  is as defined in Fig. 1 (0.507, 0.417, 0.348, 0.257, 0.170 m). (ii)  $d = 6.40$  cm. (iii)  $C_D = (D_{AB} - D_B)/(\frac{1}{2}\rho U^2 \delta)$ .  $\delta$  is projected area of cylinder and end caps *not* bars. (iv)  $\delta = 330.2, 322.5, 278.3, 220.1, 165.0$  cm<sup>2</sup> for tests 1 through 5.

the Reynolds number ranges. In Fig. 4,  $C_D$  is plotted against  $l/d$  at a particular value of  $Re$  ( $\approx 8.8 \times 10^4$ ), the graph also includes for reference the measured drag coefficients of finite-aspect-ratio circular cylinders at about the same  $Re$ . It appears that perforation increases  $C_D$  by about 20% at aspect ratios between 3 and 8.

Since the flow around a finite-aspect-ratio cylinder is highly three-dimensional, it is not possible to infer the drag of a perforated circular cylinder of length  $l$  by subtracting the drag at the end caps and supporting bar,  $D_{CB}$ , from  $D_{AB}$ . (If one makes this erroneous assumption, one finds that the end-caps' drag varies from about 1/10 to 1/4 of  $D_A$ .)

If one uses the results in Table 1 to estimate  $C_D$  when the aspect ratio  $l/d \rightarrow \infty$ , by assuming that the ratio of  $C_D$  for a perforated to an unperforated cylinder remains constant, one finds that at  $Re \approx 8.8 \times 10^4$ , where  $C_D$  for the latter is about 1.2,  $C_D$  for a long perforated cylinder is about 1.44. This is likely to be an overestimate of  $C_D$  for the damper when  $l/d \rightarrow \infty$  because end effects are usually more serious for solid than porous obstacles.

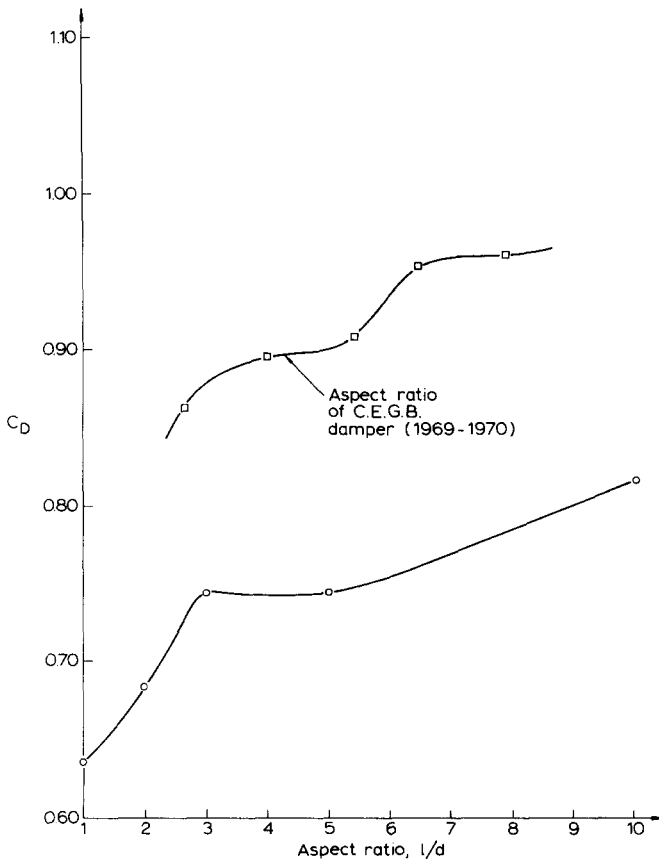


Fig. 4. Drag coefficient  $C_D$  for the aerodynamic damper (corrected for drag of the supporting bar) as a function of aspect ratio  $l/d$  at one Reynolds number  $8.8 \times 10^4$ , points denoted by  $\square$ . Points denoted by  $\circ$  are values of  $C_D$  for finite-aspect-ratio circular cylinders quoted by Goldstein [6].

### 3.2 Flow visualization

The wool tufts attached to the damper showed that at  $Re\ 1-0.2 \times 10^5$ , the air flowed right through the damper; there was no reverse flow entering on the downwind side. Wool tufts showed a region of strong eddying and intermittent back flow extending to about 5 or 6 diameters downwind. Low-speed smoke and dye visualization (Figs. 5a, 5b) showed how the fluid enters and turns outwards from the flow direction. It then develops into eddies on each side of the wake, which seem to be of small scale and independent of each other quite unlike those behind a solid cylinder.

## 4. Discussion and conclusion

We find that the drag of a finite-aspect-ratio perforated cylinder is greater by about 20% than that of the same aspect-ratio solid cylinder. By comparison,

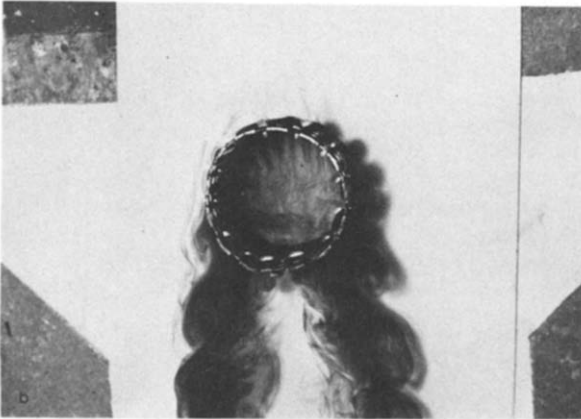
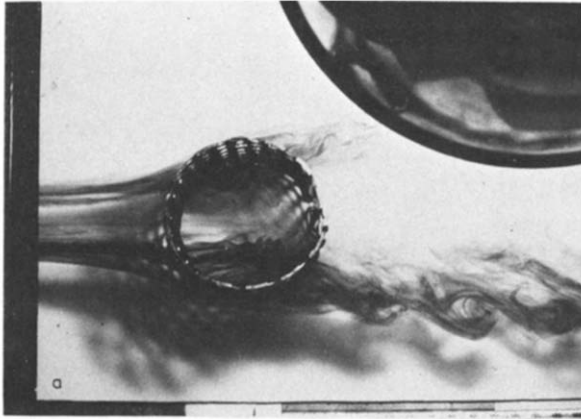


Fig. 5. Flow visualization experiments of the perforated cylinder in water. A quantity of dye is released upstream. (a) Note the flow through the cylinder. (b) Note the small scale and lack of correlation between the vortices.

a long perforated fence with the same (60%) open-area ratio ( $\beta$ ) shows a 50% reduction in its drag [1]. A possible explanation of this difference is that the drag of a perforated cylinder if  $(1 - \beta) \ll 1$  is roughly equal to the drag of the front half ( $\frac{1}{2}\rho U^2(1 - \beta)d$  per unit length) plus the drag of the back half which, since the flow passes *through* the cylinder, is about equal to or less than  $\frac{1}{2}\rho U^2(1 - \beta)d$ . Therefore, the total drag is about  $\frac{1}{2}\rho U^2 2(1 - \beta)d$ . Applying this argument to a porosity about 0.6 is questionable, but it shows how the combined drags of the front and rear faces (each of which is less than for fences of the same dimensions) can add together to produce a higher drag than a solid cylinder (if  $\beta > 0.5$ ). More detailed calculations and measurements (at difference  $\beta$ ) are certainly necessary.

The measured coefficient for the damper of 0.9 is less than the value of 1.5 assumed by Hunt and Richards [3] in their calculations of the effects of aerodynamic dampers. These measurements were confirmed by later measure-

ments of Hillier at the Central Electricity Research Laboratories [7].

The low intensity and lack of transverse correlation of the vortex shedding in the flow-visualization studies certainly bears out the qualitative tests of behaviours of full-scale aerodynamic dampers in transverse winds by Hunt and Rowbottom [8] in which no tendency to develop transverse oscillations was observed.

### Acknowledgement

We are grateful to Mr. Surey and Mr. Flaxman for help with construction of the aerodynamic dampers and to Mr. Cairns for help with conducting the experiment.

J.C.R. Hunt is grateful to North Carolina State University Department of Geo-Sciences and the Environmental Protection Agency for their hospitality and support while this note was written.

### References

- 1 I. Castro, Wake characteristics of two-dimensional perforated plates perpendicular to an air stream, *J. Fluid Mech.*, 46 (1971) 59.
- 2 J. Counihan, J.C.R. Hunt and P.S. Jackson, Wakes behind two-dimensional surface obstacles in turbulent boundary layers, *J. Fluid Mech.*, 64 (1974) 529.
- 3 J.C.R. Hunt and D.J.W. Richards, Overhead line oscillations and the effect of aerodynamic dampers, *Proc. Inst. Elec. Engrs.*, 116 (1969) 1869.
- 4 D.E. Walshe, Wind tunnel investigations of the dynamic behaviour of some tall stacks and gas-turbine exhaust towers. *Symp. Wind Effects on Buildings and Structures*; Loughborough University of Technology, 1968.
- 5 C.E. Hopley and M.J. Tunstall, A fast response anemometer for measuring the turbulence characterisation of the natural wind. *J. Phys. E: Sci. Instrum.*, 4 (1971).
- 6 S. Goldstein, *Modern Developments in Fluid Dynamics*, Oxford University Press, 1938, pp. 419, 439.
- 7 R. Hillier, Drag forces on aerodynamic dampers for overhead power lines. C.E.R.L. Note RD/L/N235/73, 1973, 489.
- 8 J.C.R. Hunt and M.D. Rowbottom, Icing test of the C.E.R.L. aerodynamic damper RD/L/M 255, 1969.